



HAL
open science

Accurate Lithium-ion battery parameter estimation with continuous-time system identification methods

Bing Xia, Xin Zhao, Raymond de Callafon, Hugues Garnier, Truong Nguyen, Chris Mi

► To cite this version:

Bing Xia, Xin Zhao, Raymond de Callafon, Hugues Garnier, Truong Nguyen, et al.. Accurate Lithium-ion battery parameter estimation with continuous-time system identification methods. *Applied Energy*, 2016, 179, pp.426-436. 10.1016/j.apenergy.2016.07.005 . hal-01346584

HAL Id: hal-01346584

<https://auf.hal.science/hal-01346584>

Submitted on 25 Oct 2023

HAL is a multi-disciplinary open access archive for the deposit and dissemination of scientific research documents, whether they are published or not. The documents may come from teaching and research institutions in France or abroad, or from public or private research centers.

L'archive ouverte pluridisciplinaire **HAL**, est destinée au dépôt et à la diffusion de documents scientifiques de niveau recherche, publiés ou non, émanant des établissements d'enseignement et de recherche français ou étrangers, des laboratoires publics ou privés.

Accurate Lithium-ion battery parameter estimation with continuous-time system identification methods

Bing Xia^{a,b}, Xin Zhao^c, Raymond de Callafon^c, Hugues Garnier^{d,e}, Truong Nguyen^b, Chris Mi^{a,*}

^a*Department of Electrical and Computer Engineering, San Diego State University, 5500 Campanile Drive, San Diego, CA 92182, USA*

^b*Department of Electrical and Computer Engineering, University of California San Diego, 9500 Gilman Dr., La Jolla, CA 92093, USA*

^c*Department of Mechanical and Aerospace Engineering, University of California San Diego, 9500 Gilman Dr., La Jolla, CA 92093, USA*

^d*University of Lorraine, CRAN, UMR 7039, 2 rue Jean Lamour, 54519 Vandoeuvre-les-Nancy, France*

^e*CNRS, CRAN, UMR 7039, France*

Abstract

The modeling of Lithium-ion batteries usually utilizes discrete-time system identification methods to estimate parameters of discrete models. However, in real applications, there is a fundamental limitation of the discrete-time methods in dealing with sensitivity when the system is stiff and the storage resolutions are limited. To overcome this problem, this paper adopts direct continuous-time system identification methods to estimate the parameters of equivalent circuit models for Lithium-ion batteries. Compared with discrete-time system identification methods, the continuous-time system identification methods provide more accurate estimates to both fast and slow dynamics in battery systems and are less sensitive to disturbances. A case of a 2nd-order equivalent circuit model is studied which shows that the continuous-time estimates are more robust to high sampling rates, measurement noises and rounding errors. In addition, the estimation by the conventional continuous-time least squares method is further improved in the case of noisy output measurement by introducing the instrumental variable method. Simulation and experiment results validate the analysis and demonstrate the advantages of the continuous-time system identification methods in battery applications.

Keywords: Lithium-ion battery, Equivalent circuit model, Battery management system, Continuous-time system identification, Instrumental variable

1. Introduction

Lithium-ion batteries have been regarded as a promising candidate for energy storage in electric vehicles due to their acceptable energy and power density compared to other types of energy storage devices [1]. To ensure safe and reliable operation of electric vehicles, the basic conditions of battery packs need to be monitored by the battery management systems (BMS), including voltage, current and temperature. Moreover, some essential states of the batteries also need to be estimated by BMSs, such as state of charge (SoC), state of health (SoH), and state of power (SoP). Since these states are usually associated with complex electrochemical reactions and cannot be directly measured by physical sensors, researchers need to refer to model-based estimation algorithms.

Among the most commonly applied modeling approaches, the electrochemical model provides high accuracy in estimation since it originates from the first principles of underlying electrochemistry. However, the accurate estimation is achieved at the cost of high complexity in data processing, which requires a significant amount of memory space and computational power to cope with partial differential equations and unknown parameters. This makes this method impractical in real-time applications.

In contrast, the equivalent circuit model (ECM) is widely accepted in the application level because of its simplicity and ease in online implementation. Equivalent circuit modeling utilizes the system identification techniques to relate the input and output behavior of the battery with circuit elements [2, 3]. An n^{th} -order ECM of Lithium-ion batteries is shown in Fig. 1. The n -RC networks can be interpreted as various time domain characteristics of the physical processes and chemical reactions within the battery cell, the series resistance R_0 is the internal resistance of the battery, and the voltage source represents the electrochemical equilibrium potential at different states, also known as open circuit voltage (OCV) [4].

All the aforementioned ECM parameters change as SoC changes, but the parameters can be regarded as constant when SoC variation is small, especially in the carefully designed character-

*Corresponding author

Email address: cmi@sdsu.edu (Chris Mi)

¹Tel.: +1 (619) 594 3741; fax: +1 (619) 594 2654 (Chris Mi)

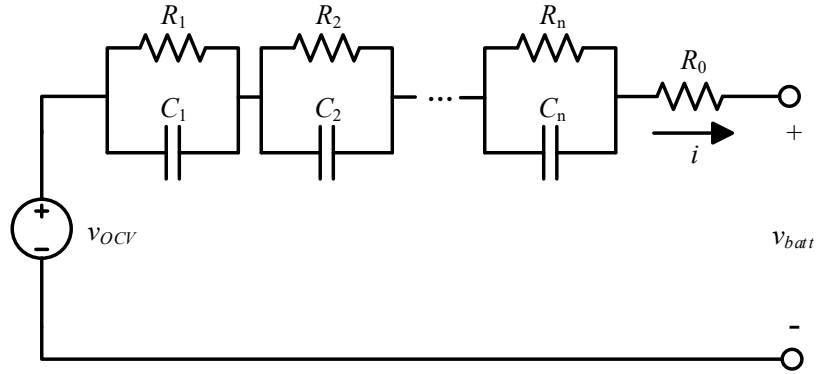


Figure 1: n^{th} order ECM for Lithium-ion batteries.

ization profiles. The battery characterization determines the best estimates of all the parameters at different SoCs. In general, the OCV is obtained by experiments, and the current and voltage responses in the hybrid pulse power characterization (HPPC) test are used to determine the values of n-RC networks and R_0 at different SoCs [5, 6, 7, 8].

Different parameter identification methods can be employed to determine the unknowns. The most common approach uses the so-called indirect approach where the parameters of an equivalent discrete-time model are first estimated from which the continuous-time parameters are then derived in a second step. Numerical searching methods utilize global/local searching algorithms to find the best fit parameters, among which the genetic algorithm (GA) and particle swarm optimization are widely applied [9, 10]. The disadvantages of such methods are: 1) the convergence to global optimization is not guaranteed given perturbations, and the result is sensitive to initial condition selection; 2) a constant searching time is not assured, which limits their application in real-time. A more robust method is to use curve fitting tools to fit constant current charging or rest periods of experiment data with exponential functions [11]. The limitation of this method lies in its ignorance of dynamic inputs in tests, thereby resulting into large voltage errors when dynamic inputs are applied. The standard discrete-time least squares (DT LS) method results in

1
2
3 the best estimation of battery parameters with both static and dynamic inputs in terms of minimiz-
4 ing the residual. The DT LS method is faster and requires less memory than numerical searching
5 methods. It has been adapted to recursive least squares (RLS) methods and RLS methods with
6 forgetting factor for online estimation [12, 13, 14, 15].
7
8

9
10 As the wide application of the discrete-time model identification in Lithium-ion batteries, re-
11 searchers have encountered a limitation that the sampling time needs to be chosen with special care.
12 If the sampling time is too large, information on the fast dynamics will be lost, whereas too small a
13 sampling time will result numerical problems, that is, the discrete poles accumulate within a small
14 area close to the boundary of the unit circle [16]. Since the battery system is a typical stiff system
15 with both fast and slow dynamics [17], the selection of sampling time is extremely difficult: rapid
16 sampling is required to capture the fast dynamics, however, it will lead to large discrepancies in
17 parameter estimation due to the existence of slow dynamics [18, 19]. Given limited storage res-
18 olution, when the discrete poles are closer to the stability boundary, the discrete system is more
19 prone to numerical precision of the parameters and the location of the discrete poles [20]. It is also
20 concluded by simulation in [21] that the sensitivities to disturbance of the resistance and capaci-
21 tance values in the RC networks increase quasi-linearly as sampling time decreases, which brings
22 difficulties in accurate system identification.
23
24
25
26
27
28
29
30
31
32
33
34
35

36 The direct continuous-time system identification has been studied as opposed to the indirect
37 discrete-time system identification [22, 23]. Compared with discrete-time identification meth-
38 ods, the advantages of the continuous-time identification methods are 1) the physical world is
39 continuous and it provides good insight of system properties; 2) the continuous-time identification
40 method avoids discretization that gives rise to undesired high sensitivity issues, and thus can better
41 deal with stiff systems [24]. More detailed differences between continuous-time and discrete-time
42 identification are provided in [18][25].
43
44
45
46
47
48

49 To the authors' best knowledge, the continuous-time approaches have not been analyzed and
50 compared with discrete-time identification methods in battery applications. The novelty of this
51 paper is 1) the continuous-time system identification methods are utilized to identify system pa-
52 rameters of Lithium-ion batteries; 2) the advantages of continuous-time system identification are
53 demonstrated in detail by analytical analysis, simulation and experiment; 3) The instrumental vari-
54
55
56
57
58

able (IV) method is applied to improve the basic continuous-time least squares estimates. In this paper, the continuous-time and discrete-time n^{th} -order ECM are first introduced. Then the system identifiability and sensitivity of the two methods are compared and discussed. Next, a case is studied to identify the parameters of a 2nd-order ECM by continuous-time system identification methods. The continuous-time least squares solution is obtained after a state variable filter (SVF) is applied to pre-process the sampled data, and the estimation is further improved with the IV based estimator for coping with the measurement noise. Simulation and experiment results agree with the analysis and demonstrate the advantages of continuous-time parameter estimation methods in real battery applications.

2. Parameter identification of continuous-time and discrete-time battery models

2.1. Continuous-time battery model

The continuous-time transfer function of the n^{th} -order ECM depicted in Fig. 1 can be written as

$$\begin{aligned} H(s) &= \frac{V_{OCV}(s) - V_{batt}(s)}{I(s)} = \frac{V(s)}{I(s)} \\ &= \frac{R_1}{R_1 C_1 s + 1} + \frac{R_2}{R_2 C_2 s + 1} + \cdots + \frac{R_n}{R_n C_n s + 1} + R_0 \end{aligned} \quad (1)$$

where $V_{OCV}(s) = \mathcal{L}\{v_{OCV}(t)\}$, $V_{batt}(s) = \mathcal{L}\{v_{batt}(t)\}$, $I(s) = \mathcal{L}\{i(t)\}$, and $\mathcal{L}\{\cdot\}$ is the notation for the Laplace transform.

This function can be rewritten as

$$(s^n + a_1 s^{n-1} + \cdots + a_{n-1} s + a_n) V(s) = (b_0 s^n + \cdots + b_{n-1} s + b_n) I(s) \quad (2)$$

where all the coefficients are functions of the unknown circuit parameters. Define

$$\begin{aligned} \theta &= [a_1 \quad \cdots \quad a_{n-1} \quad a_n \quad b_0 \quad \cdots \quad b_{n-1} \quad b_n]^T \\ &= f(R_1, \cdots, R_{n-1}, R_n, C_1, \cdots, C_{n-1}, C_n, R_0) \end{aligned} \quad (3)$$

where $f : \mathbb{R}^{2n+1} \rightarrow \mathbb{R}^{2n+1}$ maps the circuit parameters to the equation unknowns.

Equation (2) can be directly written into a regression form as

$$v^{(n)}(t) = \varphi(t)\theta \quad (4)$$

where $v^{(n)}(t)$ denotes the n^{th} time-derivative of $v(t) = v_{OCV}(t) - v_{batt}(t)$, and $\varphi(t)$ is the regression vector given by

$$\varphi(t) = [-v^{(n-1)}(t) \quad \cdots \quad -v(t) \quad i^{(n)}(t) \quad \cdots \quad i(t)] \quad (5)$$

In practice, the measured terminal voltage of batteries is usually contaminated by noises. Therefore, an equation error $e(t)$ is added to the given regression form. Thus a complete model is given by

$$v^{(n)}(t) = \varphi(t)\theta + e(t) \quad (6)$$

2.2. Discrete-time battery model

To obtain the discrete-time battery model, by using the correct piecewise constant assumption for the current input in HPPC tests, the zero-order hold (ZOH) equivalent of (1) can be derived by (7).

$$H(z) = (1 - z^{-1})\mathcal{Z}\left\{\frac{H(s)}{s}\right\} \quad (7)$$

where $\mathcal{Z}\{\cdot\}$ is the notation for the z -transform.

Thus the continuous-time transfer function (1) yields to

$$H(z) = \frac{V(z)}{I(z)} = \frac{R_1(1 - e^{-\frac{T_s}{R_1 C_1}})}{z - e^{-\frac{T_s}{R_1 C_1}}} + \frac{R_2(1 - e^{-\frac{T_s}{R_2 C_2}})}{z - e^{-\frac{T_s}{R_2 C_2}}} + \cdots + \frac{R_n(1 - e^{-\frac{T_s}{R_n C_n}})}{z - e^{-\frac{T_s}{R_n C_n}}} + R_0 \quad (8)$$

and it can be rewritten as

$$(1 + c_1 z^{-1} + \cdots + c_n z^{-n})V(z) = (d_0 + d_1 z^{-1} + \cdots + d_n z^{-n})I(z) \quad (9)$$

where T_s is the sampling interval, and the coefficients in (9) are functions of the unknown parameters as well as T_s . Define

$$\begin{aligned} \theta_d &= [c_1 \quad \cdots \quad c_n \quad d_0 \quad d_1 \quad \cdots \quad d_n]^T \\ &= g(R_1, \cdots, R_{n-1}, R_n, C_1, \cdots, C_{n-1}, C_n, R_0, T_s) \end{aligned} \quad (10)$$

where $g : \mathbb{R}^{2n+2} \rightarrow \mathbb{R}^{2n+1}$ maps the circuit parameters and T_s to the equation unknowns.

Similar to the continuous-time model, a regression form of (9) with a noise term $\epsilon(k)$ can be written as

$$v(k) = \varphi_d(k)\theta_d + \epsilon(k) \quad (11)$$

where

$$\varphi_d(k) = [-v(k-1) \quad \cdots \quad -v(k-n) \quad i(k) \quad i(k-1) \quad \cdots \quad i(k-n)] \quad (12)$$

and $v(k)$ denotes the sampled value of $v(t)$ at time-instant t_k .

2.3. System identifiability

The structural identifiability describes the uniqueness of parameters given a dynamic model with noise-free and persistent excitations [26, 27]. The battery system is globally identifiable if there is a unique solution θ , $\theta \in \Theta \subset \mathbb{R}^{2n+1}$, for (6) and (11); the system is locally identifiable if there are a finite number of solutions in Θ ; the system is unidentifiable if there are an infinite number of solutions in Θ .

The identifiability of Randles ECMs are discussed in [28]. The n^{th} -order ECM discussed in this paper has similar structure as that of the Randles models, except for an additional capacitor connecting in series with the RC networks. Similar derivations hold for the ECM of interest in this paper as well.

Given the continuous system transfer function as (1), if two sets of circuit parameters lead to the same transfer function of an ECM, then

$$\frac{R_1}{R_1 C_1 s + 1} + \cdots + \frac{R_n}{R_n C_n s + 1} + R_0 = \frac{R_1^*}{R_1^* C_1^* s + 1} + \cdots + \frac{R_n^*}{R_n^* C_n^* s + 1} + R_0^*, \text{ for all } s \quad (13)$$

A necessary condition for (13) to hold is

$$\left(s + \frac{1}{R_1 C_1}\right) \cdots \left(s + \frac{1}{R_n C_n}\right) = \left(s + \frac{1}{R_1^* C_1^*}\right) \cdots \left(s + \frac{1}{R_n^* C_n^*}\right), \text{ for all } s \quad (14)$$

Since an n degree polynomial is uniquely characterized by its n distinct roots, the assignments of $(-\frac{1}{R_1^* C_1^*}, \dots, -\frac{1}{R_n^* C_n^*})$ in (14) need to be the permutations of $(-\frac{1}{R_1 C_1}, \dots, -\frac{1}{R_n C_n})$. Assume the order of the distinct roots is strictly defined, i.e. $R_1 C_1 < \cdots < R_n C_n$ and $R_1^* C_1^* < \cdots < R_n^* C_n^*$. Since the functions of $1/(s + \frac{1}{R_i C_i})$ in (14) are linear independent, $R_i C_i = R_i^* C_i^*$ can be obtained and consequently $R_i = R_i^*$ from (13) for $i = 1, 2, \dots, n$. Therefore, all the parameters in the model structure of (1) are uniquely determined. The one-to-one mapping of f in (3) ensures the uniquely determined θ in the reparametrization.

Similar derivation holds for discrete time ECM identifiability. Therefore, the conclusion can be drawn that both continuous-time and discrete-time n^{th} -order ECMs are globally identifiable when the order of the RC networks is strictly defined.

2.4. Sensitivity of discrete-time model poles

The time-constants of an ECM describe essential system properties of the circuit. Physically, they give the time domain characteristics of voltage variations due to different chemical or physical processes upon charge and discharge. The time-constants τ_i in the ECM are calculated by

$$\tau_i = R_i C_i, i = 1, 2, \dots, n \quad (15)$$

Note that the time-constants are closely related to the eigenvalues, or pole locations of the system as

$$\tau_i = \frac{1}{|\lambda_i|}, i = 1, 2, \dots, n \quad (16)$$

where λ_i is the i^{th} eigenvalue of the system.

In order to characterize the fast dynamics of a system, the sampling frequency should be high enough. A rule of thumb [19] is to select a sampling time such that

$$f_s \geq 2 \times \frac{1}{\tau_{\min}} \Leftrightarrow |\lambda_{\max}| T_s \leq \frac{1}{2} \quad (17)$$

where λ_{\max} is the largest eigenvalue, τ_{\min} is its corresponding smallest time-constant in the system, T_s is the sampling time and f_s is the sampling frequency. In practical applications, the sampling frequency f_s is usually set to be higher than the boundary value of $2/\tau_{\min}$ to ensure sufficient sampling.

However, a high sampling rate gives rise to undesirable sensitivity issues as illustrated in Fig. 2. It is well known that the negative real poles in the s -domain map to the interval between the origin and (1, 0) on the real axis of z -domain by (18). As $\lambda_i T_s \rightarrow 0$, the poles in the z -domain approaches (1, 0).

$$z_i = e^{\lambda_i T_s} \quad (18)$$

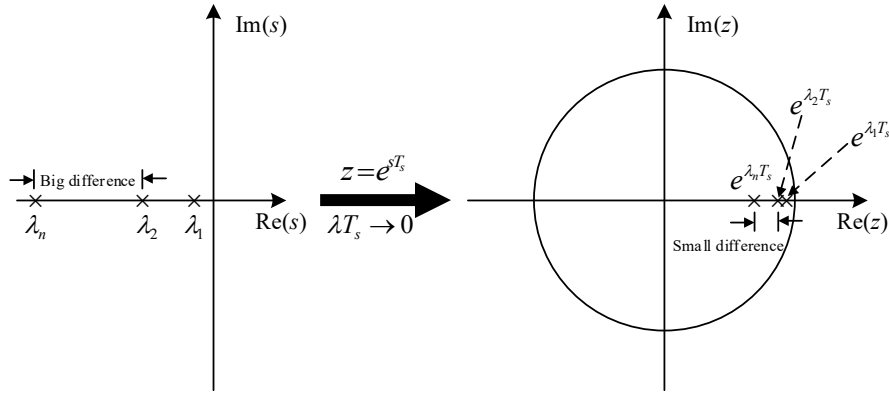


Figure 2: Discrete pole converges to (1, 0) in z -plane as $\lambda T_s \rightarrow 0$.

Given (16), the sensitivity of the continuous-time model time-constant with respect to z -domain pole location can be derived as (19).

$$S = \left| \frac{z}{\tau} \frac{\partial \tau}{\partial z} \right| = \left| \frac{e^{-\frac{T_s}{\tau}}}{\tau} \frac{\partial \tau}{\partial e^{-\frac{T_s}{\tau}}} \right| = \frac{e^{-\frac{T_s}{\tau}}}{\tau} \frac{\tau^2}{T_s e^{-\frac{T_s}{\tau}}} = \frac{1}{|\lambda| T_s} = \tau f_s \quad (19)$$

The result shows that the sensitivity is the product of sampling frequency and time-constant. Without considering the hardware cost, high sampling frequency is desired so that the discrete-time system is a good approximation of the continuous-time system. However, equation (19) implies that faster sampling yields to higher sensitivity of the discrete-time model identification to external disturbances and computation errors.

One can also observe from (19) that the sensitivity is larger for larger time-constants. In a practical on-board battery monitoring system, the sampling frequency can be 100 Hz, and typical time-constant values for 2nd-order ECMs are 30 s and 1,000 s [29], thus the sensitivities can be locally as high as 3,000 and 100,000 respectively. It indicates that a small variation in z -domain pole estimation leads to a significant change in time-constant estimation. In the extreme condition, as $\lambda T_s \rightarrow 0$, the sensitivity goes to infinity.

It is important to state that such a sensitivity issue stems from the discretization process, and it does not exist in the continuous-time model identification cases.

2.5. Prescaling in fixed-point storage

Most on-board vehicular microprocessors use fixed-point data storage systems. Such representation limits the information that can be stored during calculation due to precision loss and overflow.

In the continuous-time model identification process, given the stiffness of battery systems, the time-constants vary in one or two orders of magnitude. Since the to-be-estimated coefficients are closely related to the multiplication of different pole locations, these coefficients can be different in several orders of magnitude. If the magnitude of the coefficients is too small, it will lead to big discrepancies in storage, because of the fixed minimum resolution. In order to solve this problem, a parameter prescaling technique is used to maintain the coefficients in the same order of magnitudes, as

$$\tilde{\theta} = U\theta \quad (20)$$

where the prescaling matrix

$$U = \begin{bmatrix} u_1 & 0 & \cdots & 0 \\ 0 & u_2 & \ddots & \vdots \\ \vdots & \ddots & \ddots & 0 \\ 0 & \cdots & 0 & u_{2n+1} \end{bmatrix} \quad (21)$$

and θ is the parameter vector defined in (3).

For instance, if b_n in θ has a magnitude in the order of 10^{-9} , whereas the processor is 16 bits, i.e. the resolution is $2^{-16} = 1.5 \times 10^{-4}$, it is impossible to store b_n in such processor for any further calculation. In this case, u_{2n+1} in U can be set to 10^9 such that $u_{2n+1}b_n$ can be stored properly. Then θ can be retrieved by

$$\theta = U^{-1}\tilde{\theta} \quad (22)$$

In the discrete-time model identification, the dominating poles are close to 1, thus the to-be-estimated coefficients have similar order of magnitudes. Therefore the prescaling is not necessary.

2.6. Summary of the differences between continuous-time and discrete-time model identification

The major differences of continuous-time and discrete-time model identification are listed in Table 1. In summary, the advantages of continuous-time over discrete-time model identification

1
2
3 are
4
5

- 6 a) The identified parameters do not change as T_s changes, as shown in (3) and (10), where θ_d
7 is related to T_s .
8
9
10 b) High sampling rate to avoid information loss does not lead to undesired high sensitivity
11 issues.
12
13 c) The continuous-time approach includes inherent filtering, so it is more robust to measure-
14 ment noises. This is to be discussed in detail in Section 3.
15
16 d) Additional advantages have been recently discussed and illustrated in [18] and [23].
17
18
19
20
21
22

23 The disadvantage of continuous-time model identification are
24

- 25 a) The prescaling is required for application in fixed-point storage.
26
27
28 b) More computational power is needed to filter the input/output. This is to be discussed in
29 Section 3.
30
31
32

33 **Table 1:** Major differences between discrete-time (DT) and continuous-time (CT) model identification.
34
35

	DT	CT
a)	Uses z -transform.	Uses Laplace transform.
b)	Deals with difference equations.	Deals with differential equations.
c)	θ_d changes as T_s changes.	θ remains unchanged.
d)	DT models are derived from CT, and go back to CT.	Remains as CT.
e)	Small T_s or large τ make the system identification sensitive to rounding errors and noises.	No undesired sensitivity issues.
f)	Does not have prefiltering.	Has inherent prefiltering.
g)	Works easily with fixed-point storage.	Requires prescaling in fixed-point storage.
h)	Requires less computation.	Requires more computation in filtering.

3. Continuous-time identification of battery models

3.1. Conventional least squares based SVF method

The continuous-time model parameter can be obtained from the least squares solution of θ in (6). However, the time-derivatives of the input and output are usually not measured. One traditional approach to handle the time-derivatives measurement problem is to use the state variable filter (SVF) method (see e.g. [16]), which generates filtered (smoothed) versions of the required time-derivatives. A typical SVF is in the form of

$$L_n(s) = \left(\frac{\alpha}{s + \alpha} \right)^n \quad (23)$$

where n is the highest system order, and α determines the cut-off frequency of the SVF. The choice of α is recommended to be slightly higher than the estimated bandwidth of the system [16]. Applying the SVF to (6) yields the linear model as (24).

$$v_{svf}^{(n)}(t) = \varphi_{svf}(t)\theta + e'(t) \quad (24)$$

where $\varphi_{svf}(t) = [-v_{svf}^{(n-1)}(t) \ \cdots \ -v_{svf}(t) \ i_{svf}^{(n)}(t) \ \cdots \ i_{svf}(t)]$, $v_{svf}^{(n)}(t) = \mathcal{L}^{-1}\{s^n L_n(s)V(s)\}$, $i_{svf}^{(n)}(t) = \mathcal{L}^{-1}\{s^n L_n(s)I(s)\}$, and $\mathcal{L}^{-1}\{\cdot\}$ denotes the inverse Laplace transform.

Based on N sampled measurements of both input and output signals at time instants t_k , $k = 1, \dots, N$, the continuous-time least squares based state variable filter (CT LSSVF) estimator of θ is expressed as

$$\hat{\theta}_{lssvf} = \left[\sum_{k=1}^N \varphi_{svf}^T(t_k) \varphi_{svf}(t_k) \right]^{-1} \sum_{k=1}^N \varphi_{svf}^T(t_k) v_{svf}^{(n)}(t_k) \quad (25)$$

3.2. Improved instrumental variable based SVF method

The least squares solution is unbiased when the equation error is uncorrelated to the regressor, whereas this is usually not true in real applications. In other words, $\hat{\theta}_{lssvf}$ converges to the true parameter θ_0 with the assumption of $E[\varphi_{svf}^T(t_k)e'(t_k)] = 0$, but the least squares regressor $\varphi_{svf}(t)$ contains the measured output voltage, which correlates with $e'(t)$ by (24). In order to make the continuous-time parameter identification consistent for correlated equation errors, the instrumental variable (IV) method is introduced. The main idea of the IV method is to find an instrument

1
2
3
4 $\zeta(t_k)$ whose components are uncorrelated with $e'(t_k)$, i.e. $\frac{1}{N} \sum_{k=1}^N \zeta_{svf}^T(t_k) e'(t_k) = 0$ [30]. The most
5 common IV method utilizes an auxiliary model to generate a noise-free estimate of output, as
6

$$7 \quad \zeta_{svf}(t_k) = [-w_{svf}^{(n-1)}(t_k) \quad \cdots \quad -w_{svf}(t_k) \quad i_{svf}^{(n)}(t_k) \quad \cdots \quad i_{svf}(t_k)] \quad (26)$$

8
9 where $w_{svf}(t_k)$ is the noise-free estimate of voltage calculated by
10
11

$$12 \quad w_{svf}(t_k) = \mathcal{L}^{-1}\{L_n(s)H(s, \hat{\theta}_{lsvf})I(s)\} \quad (27)$$

13
14
15
16
17 The continuous-time instrumental variable based state variable filter (CT IVSVF) estimator of
18 θ is given as
19

$$20 \quad \hat{\theta}_{ivsvf} = \left[\sum_{k=1}^N \zeta_{svf}^T(t_k) \varphi_{svf}(t_k) \right]^{-1} \sum_{k=1}^N \zeta_{svf}^T(t_k) v_{svf}^{(n)}(t_k) \quad (28)$$

21
22
23
24 The flow chart for the implementation of n^{th} -order CT IVSVF battery parameter estimator is
25 summarized in Fig. 3.
26

27
28 It can be noticed that there is no further assumption or limitation of the operating conditions of
29 batteries in continuous-time identification, so long as the battery is in its defined normal operating
30 range. In addition, when dealing with stiff systems, the continuous-time identification method
31 does not require as high storage resolution as discrete-time identification does, because it does
32 not involve numerically dedicate transformation. Therefore, the continuous-time identification
33 methods are expected to have better performance over discrete-time methods, especially when the
34 system is stiff and the storage resolution is limited.
35
36
37
38
39
40
41

42 3.3. Model parameterization of the 2nd-order ECM

43
44 Based on the analysis in the previous sections, the continuous-time identification methods can
45 be applied to an ECM with any order. In the following sections, the 2nd order ECM is selected
46 because it is the simplest form to present a stiff system. Other than that, [31] concludes that
47 the 2nd order ECM is an optimum choice for implementation of most battery energy and power
48 management strategies.
49
50
51
52
53
54
55
56
57
58
59
60
61
62
63
64
65

The continuous-time parameters for the 2nd-order ECM identification are given as

$$\begin{aligned}
 a_1 &= \frac{1}{R_1 C_1} + \frac{1}{R_2 C_2} \\
 a_2 &= \frac{1}{R_1 C_1 R_2 C_2} \\
 b_0 &= R_0 \\
 b_1 &= R_0 \left(\frac{1}{R_1 C_1} + \frac{1}{R_2 C_2} \right) + \frac{1}{C_1} + \frac{1}{C_2} \\
 b_2 &= \frac{R_0 + R_1 + R_2}{R_1 C_1 R_2 C_2}
 \end{aligned} \tag{29}$$

For comparison purposes, the discrete-time parameters are given as

$$\begin{aligned}
 c_1 &= -(e^{-\frac{T_s}{R_1 C_1}} + e^{-\frac{T_s}{R_2 C_2}}) \\
 c_2 &= e^{-(\frac{T_s}{R_1 C_1} + \frac{T_s}{R_2 C_2})} \\
 d_0 &= R_0 \\
 d_1 &= -R_0 \left(e^{-\frac{T_s}{R_1 C_1}} + e^{-\frac{T_s}{R_2 C_2}} \right) + R_1 (1 - e^{-\frac{T_s}{R_1 C_1}}) + R_2 (1 - e^{-\frac{T_s}{R_2 C_2}}) \\
 d_2 &= R_0 e^{-(\frac{T_s}{R_1 C_1} + \frac{T_s}{R_2 C_2})} - R_1 e^{-\frac{T_s}{R_2 C_2}} (1 - e^{-\frac{T_s}{R_1 C_1}}) - R_2 e^{-\frac{T_s}{R_1 C_1}} (1 - e^{-\frac{T_s}{R_2 C_2}})
 \end{aligned} \tag{30}$$

Note that the continuous-time parameters are more complex functions of circuit parameters

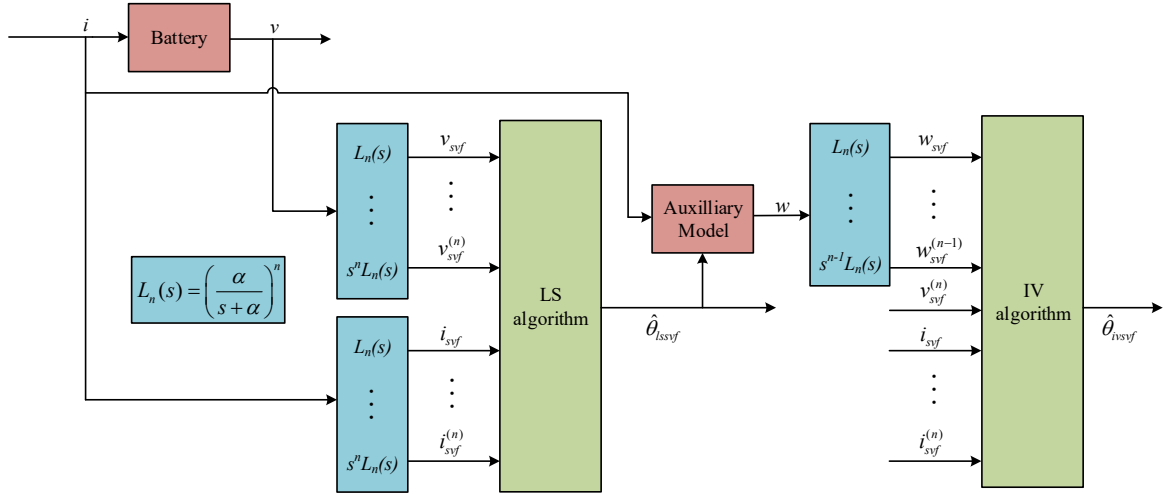


Figure 3: Implementation flow of CT IVSVF battery parameter estimator.

only, while the discrete parameters are functions of both circuit parameters and T_s , as indicated in (3) and (10).

4. Simulation results

4.1. Simulation setup

Simulations are set up in MATLAB to compare the performance of continuous-time and discrete-time identification methods. In the simulation, the circuit of interest is assumed to have $R_0 = 1 \text{ m}\Omega$, $R_1 = 0.3 \text{ m}\Omega$, $R_2 = 0.6 \text{ m}\Omega$, $\tau_1 = 30 \text{ s}$ and $\tau_2 = 1000 \text{ s}$, and the capacity of the battery is 40 Ah. It needs to be noticed that the simulated system is a typical stiff system, because it includes a fast and a slow time-constants.

The input excitation is shown in Fig. 6c. It consists of five pairs of discharge and charge pulses, each lasting for 20 s. The amplitude of the pulse pairs are 0.5C, 1.0C, 1.5C, 2.0C and 2.5C, respectively, where C is a measure of current at which a battery is discharged to its nominal capacity. The rest periods after each discharge pulses are 40 s, and the rest periods after each charge pulses are 60 s. After the five pair of pulses, a 0.5C 2% SoC discharge is applied, followed by a 1-hour rest.

Various sampling intervals are used in the simulation, which are set to be 1 s, 0.1 s, and 0.01 s, respectively. White Gaussian noises with different signal to noise ratios (SNR) are added to the voltage output in the simulation to emulate the measurement noise of the system, such that

$$v(k) = v_{det}(k) + n(k) \quad (31)$$

where v_{det} is the deterministic (or noise-free) voltage signal, $n(k)$ is the measurement noise added to the noise-free voltage signal, and $v(k)$ is the noisy voltage measurement.

The SNR is defined as

$$\text{SNR}_{\text{dB}} = 10 \log_{10} \frac{\sigma_{v_{det}}^2}{\sigma_n^2} \quad (32)$$

where $\sigma_{v_{det}}^2$ is the variance of v_{det} and σ_n^2 is the variance of the added noises. The standard deviation of noises are chosen to be 0.01 mV, 1 mV and 10 mV respectively. Therefore the corresponding SNR values are 62 dB, 22 dB and 2 dB, respectively.

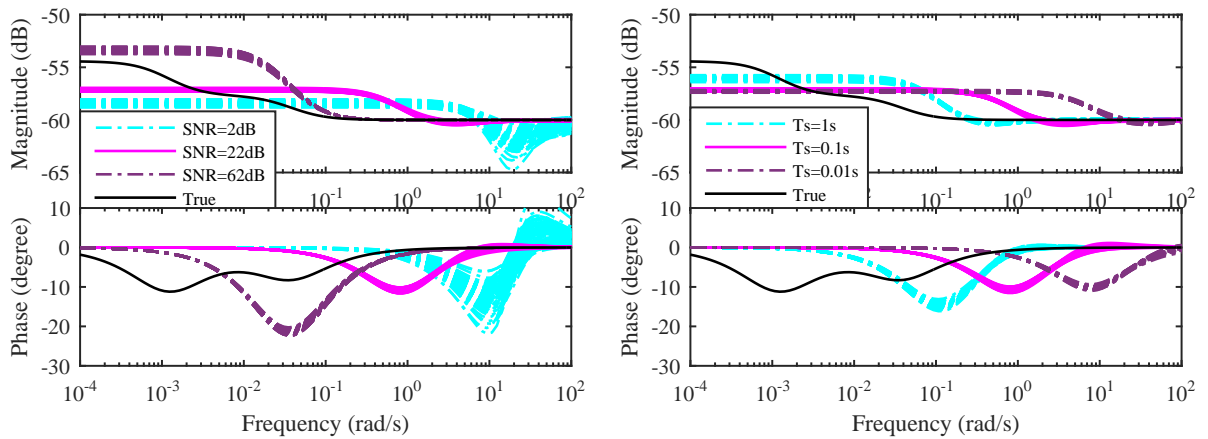
The SVF cut-off frequency is 0.01 rad/s. Unless otherwise specified, the intermediate data storage for all the simulation is 16 bits, and the prescaling technique introduced in Sec. 2.5 is applied to all simulation.

Monte Carlo simulations are used to evaluate the performance of the model identification methods, such that 100 different noise realizations are generated for each of the sampling intervals and noise levels. The Bode plots of the identified systems are presented for different methods in various conditions. Except DT LS, CT LSSVF and CT IVSVF methods, it is also interesting to see the performance of DT LS method with the same pre-filtering as in the continuous-time methods, as suggested by [12]. The Bode plots of estimated models based on discrete-time methods are presented in Fig. 4, and those based on continuous-time methods are presented in Fig. 5.

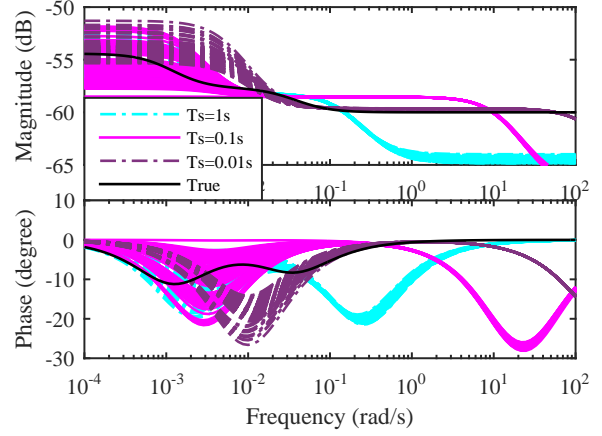
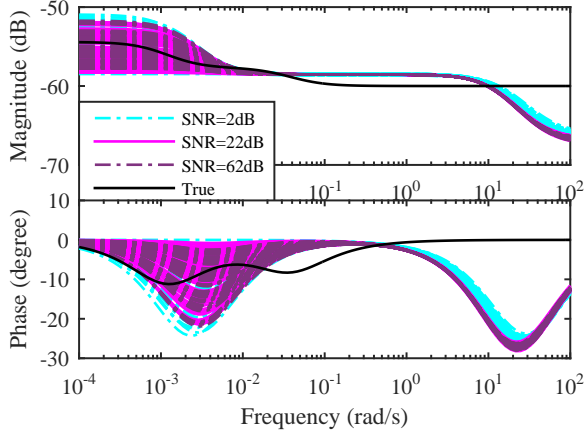
4.2. Discussion of simulation results

Fig. 4a and Fig. 4b give the Bode plots for the CT models identified by the indirect DT LS-based method. The identified models are clearly biased at the low frequency ends. As the noise level or sampling rate increases, the identified systems are more biased.

The Bode plots for the systems identified by the DT LS methods with both input and output filtering are given in Fig. 4c and Fig. 4d. The filter applied is the same as $L_2(s)$ with same cut-off frequency as SVF. It is hard to conclude solely from the two plots whether the pre-filtering improves the system identification, but at least the pre-filtering does not provide the desired system

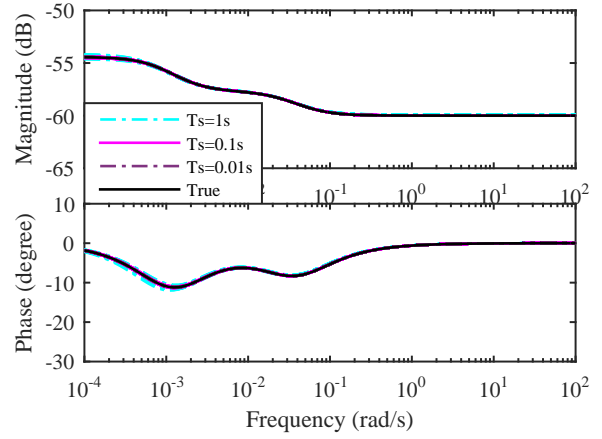
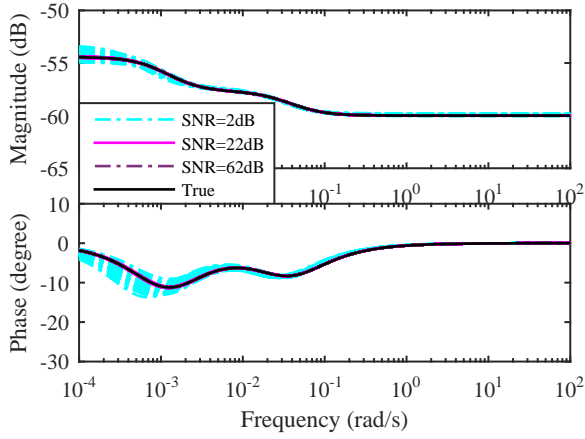


(a) DT LS method for different SNR ($T_s=0.1$ s, 16 bits). (b) DT LS method for different T_s (SNR=22dB, 16 bits).



(c) DT LS method with pre-filtering for different SNR ($T_s=0.1$ s, 16 bits).

(d) DT LS method with pre-filtering for different T_s (SNR=22dB, 16 bits).



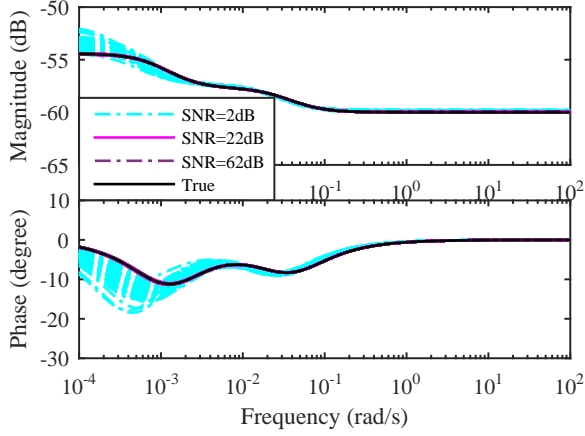
(e) DT LS method with pre-filtering for different SNR ($T_s=0.1$ s, 64 bits).

(f) DT LS method with pre-filtering for different T_s (SNR=22dB, 64 bits).

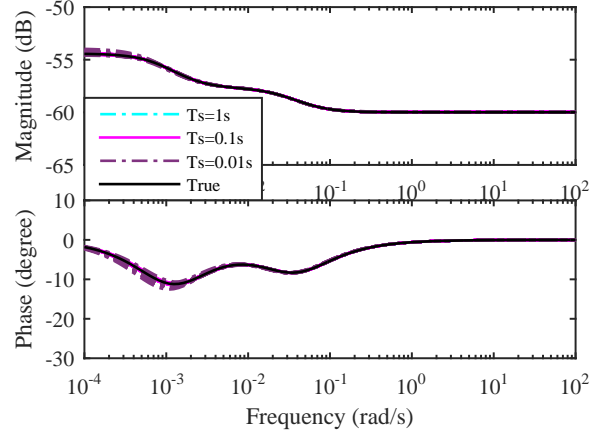
Figure 4: Monte Carlo simulation with different SNR and T_s . Bode plots of CT models from indirect DT methods.

identification. Later simulation with 64 bit storage resolution in Fig. 4e and Fig. 4f demonstrates the effectiveness of the pre-filtering in high storage resolutions. The difference in the identification performance indicates that the pre-filtering is largely influenced by the rounding errors in discrete-time identification.

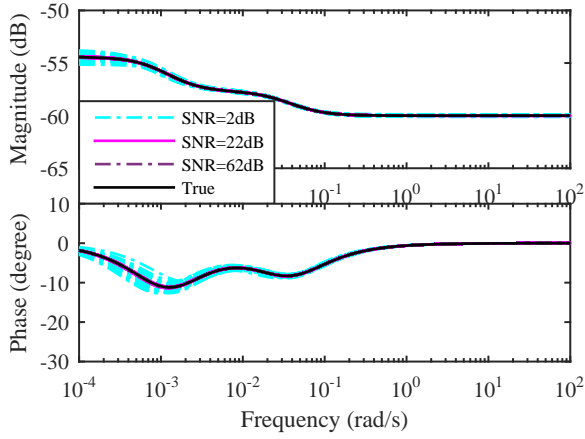
Fig. 5a and Fig. 5b present the identification results of CT LSSVF method in various conditions. The performance of system identification is remarkably improved, which is due to the application of data pre-filtering and avoidance of discretization.



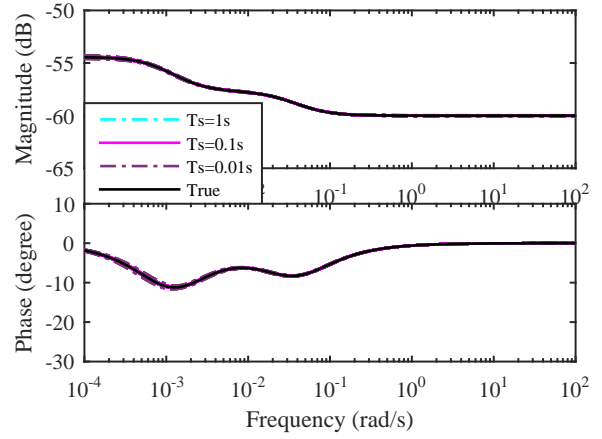
(a) CT LSSVF method for different SNR ($T_s=0.1$ s, 16 bits).



(b) CT LSSVF method for different T_s (SNR=22dB, 16 bits).



(c) CT IVSVF method for different SNR ($T_s=0.1$ s, 16 bits).



(d) CT IVSVF method for different T_s (SNR=22dB, 16 bits).

Figure 5: Monte Carlo simulation with different SNR and T_s . Bode plots of CT models from direct CT methods.

At last, Fig. 5c and Fig. 5d show that CT IVSVF identification has accurate identifications in all situations, where the Bode plots of the identified systems overlap that of the true system with a high fidelity except when the SNR is equal to 2dB when a bias can be observed in the low-frequency part of the response.

In summary, most of the indirect discrete-time identification methods lead to large discrepancies in system identification, especially in the presence of noises and small sampling intervals; the simple CT LSSVF estimates are clearly less biased due to SVF pre-filtering and low sensitivity to

Table 2: Specification of battery under test.

Material	Lithium-ion polymer
Charge/discharge capacity	40.83/40.61 Ah
Nominal voltage	3.7 V
Maximum charge voltage	4.2 V
Minimum discharge voltage	2.7 V

rounding errors, and the CT IVSVF estimates are both accurate and robust in all situation.

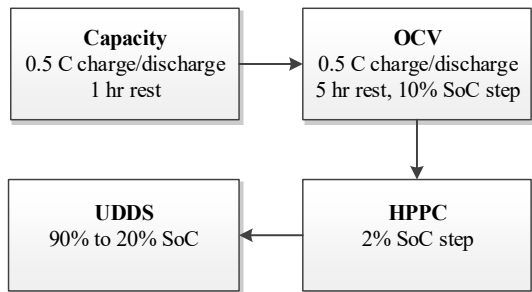
5. Experimental results

5.1. Battery tests

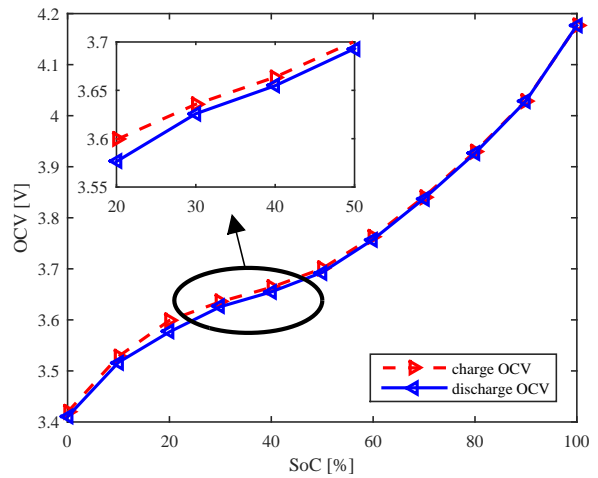
In order to identify the parameters of a Lithium-ion polymer cell, battery characterization experiments are conducted at room temperature ($22^{\circ}\text{C}\sim 25^{\circ}\text{C}$). The specification of the battery under tests is given in Table 2. The procedure of the characterization tests is shown in Fig. 6a. The sampling rate in all the experiments is 1 Hz.

The capacity test consists of three charge/discharge cycles. In each cycle, the battery is charged with a constant current of 0.5C until the terminal voltage reaches the maximum charge voltage. Then the voltage is kept at the maximum charge voltage until the charge current is below 1/20C. After that, the battery is discharged at 0.5C until the minimum discharge voltage is reached. A 1 hr rest is applied after each charge/discharge operation. The charge/discharge capacity are calculated as the average value of the three cycles.

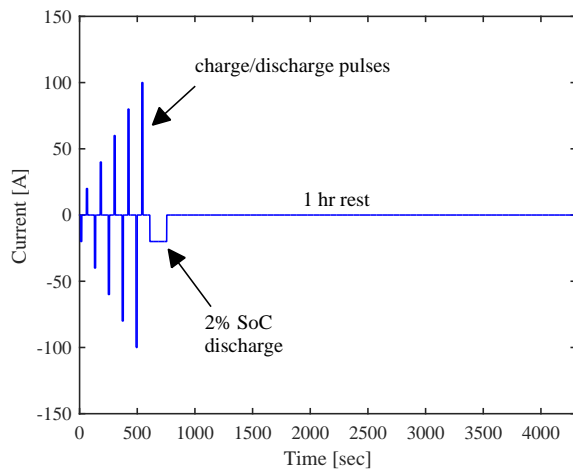
The charge/discharge OCV-SoC curves are obtained at 10% SoC step with 0.5C charge/discharge rate and 5 hr rest, as shown in Fig. 6b. It can be observed that the charge OCV curve is higher than the discharge curve due to the hysteresis effect. The maximum difference between charge/discharge curves is 22.6 mV. The average value of charge/discharge OCV curves is used in the model calculation for simplicity.



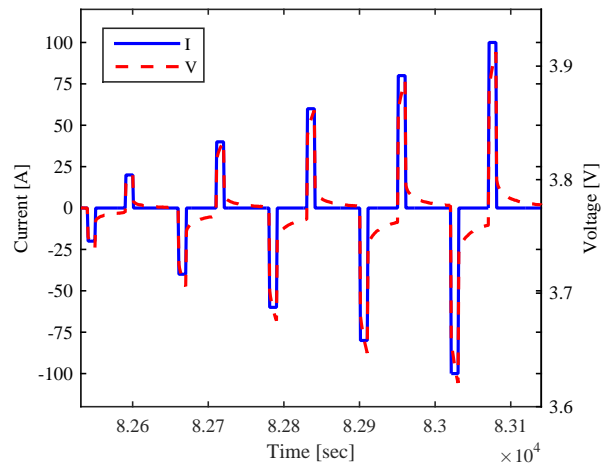
(a) Battery characterization procedure.



(b) OCV of the battery under test.



(c) HPPC test profile.



(d) HPPC pulses at SoC=50%.

Figure 6: Battery characterization and validation experiments.

The HPPC test profile is the same as mentioned in Section 4. The HPPC test is repeated between 10% and 90% SoC with 2% SoC step. The current input and voltage output of the HPPC pulses at SoC=50% are shown in Fig. 6d.

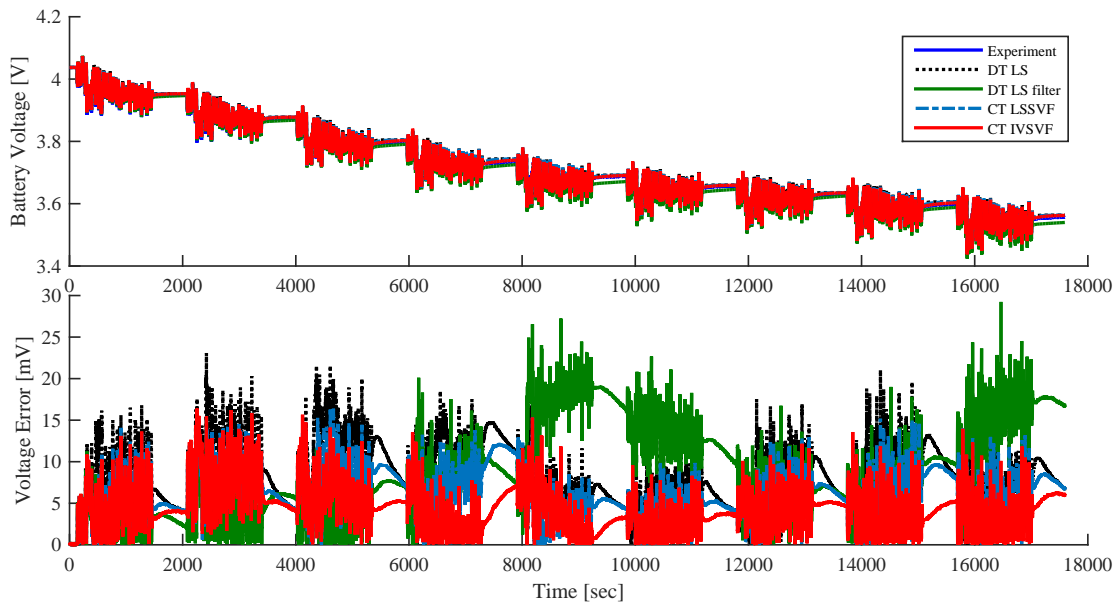
Finally, Urban Dynamometer Driving Schedule (UDDS) cycles with 10 minutes rest periods are applied consecutively to the battery cell to validate the identified model. The initial SoC for UDDS test is 90%, and the test is terminated after the first cycle when SoC drops below 20%. The current profile of UDDS is scaled such that the maximum discharge current is 100 A.

5.2. Discussion of experimental results

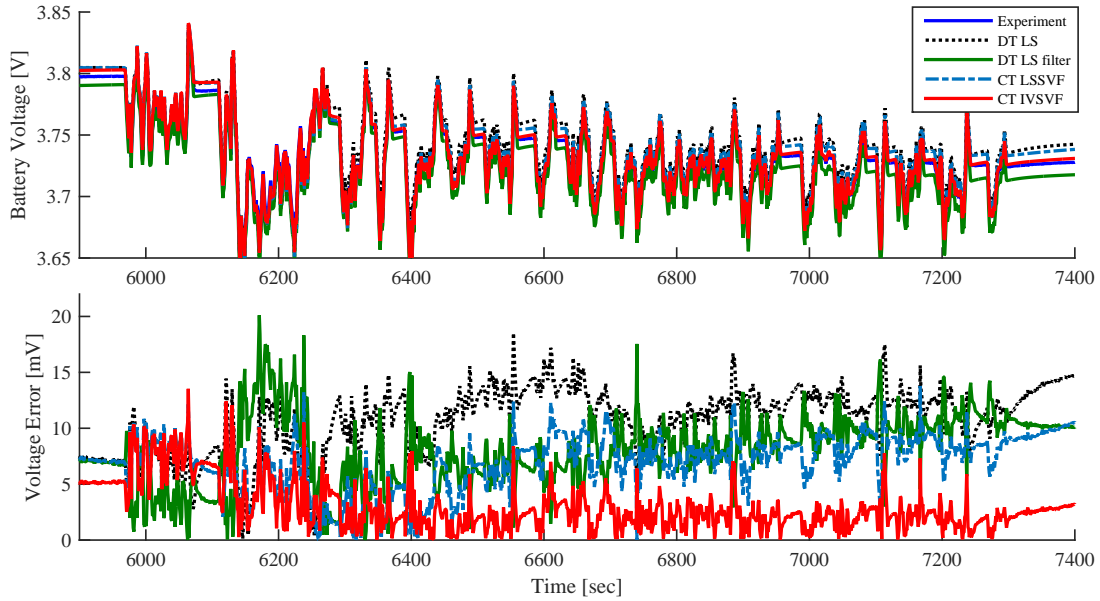
In order to demonstrate the advantages of continuous-time system identification, the performances of CT LSSVF and CT IVSVF estimators are compared with DT LS method and DT LS with pre-filtering. The cut-off frequency for both of the filters are 0.025 rad/s and the storage resolution is 16 bits.

The voltage outputs of the simulated models and experiments in UDDS are plotted in Fig. 7a, and the zoomed-in range between 5,900 s and 7,400 s are shown in Fig. 7b. The results show that

- i) The indirect discrete-time methods have the larger overall error.
- ii) The DT LS method with pre-filtering has similar noise levels to the CT LSSVF method in some of the cycles, however, the systems identified are clearly biased in the 5th, 6th and 9th cycle. The defect in robustness is mainly caused by its high sensitivity to unmodeled dynamics and colored noises in the experiment.
- iii) The two direct continuous-time identification methods have better performance over other methods. Furthermore, CT IVSVF estimator gives better estimation because the newly introduced instrumental variable is less correlated to equation error.



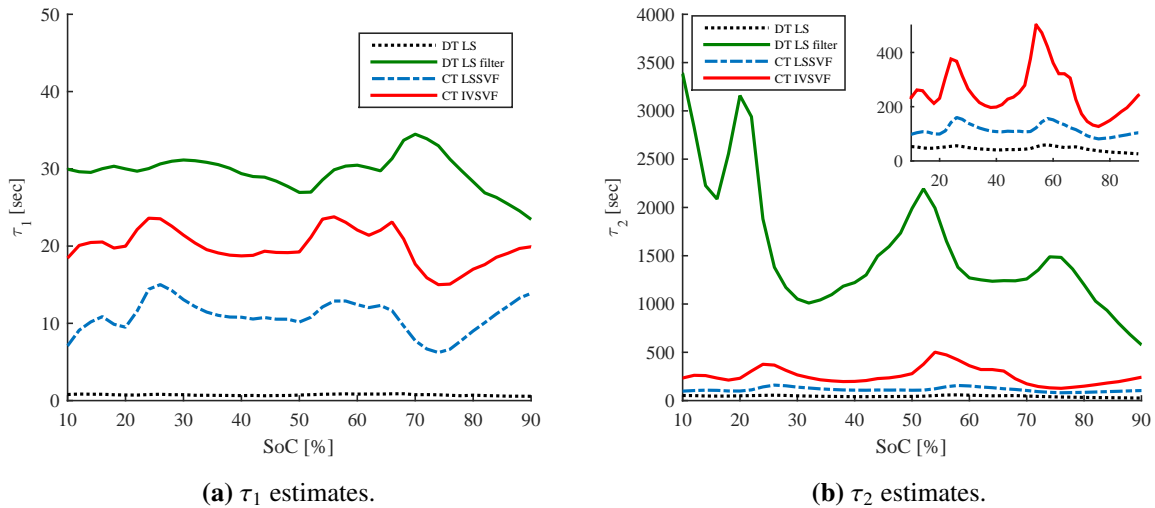
(a) Voltage values and errors across all UDDS tests.



(b) Detailed voltage values and errors for 5,900 s and 7,400 s.

Figure 7: Discrepancies of different identification methods.

Based on the findings in simulation results, the DT LS method tends to estimate the poles of the system to be larger, then the corresponding time-constants are smaller. This can be observed in Fig. 8 as well, where the time-constant estimates of DT LS are the smallest among all the methods.



(a) τ_1 estimates.

(b) τ_2 estimates.

Figure 8: Time-constant estimates from experimental data with different methods.

1
2
3
4 It needs to be noticed that DT LS presents acceptable results in experiments because the UDDS
5 cycle mainly consists of high frequency contents, where it gives reasonable identification in the
6 simulation as well. However, it has large bias in larger time-constant estimates, which will lead to
7 larger discrepancies when the input is constant. This can be visualized by its larger discrepancies
8 at beginning of rest periods between UDDS cycles.
9

10
11
12 The mean absolute error (MAE) and root mean squares error (RMSE) of the aforementioned
13 estimators within the whole experimental period are listed as in Table 3. It validates that the
14 continuous-time identification methods have better overall performance and CT IVSVF method
15 gives voltage estimations with the smallest error.
16
17
18
19
20
21

22 6. Conclusion

23
24
25 This paper has presented the advantages of continuous-time system identification methods in
26 battery ECM parameter estimation. The combination of fast dynamics induced by charge transfer
27 and slow dynamics from diffusion causes the dynamics of a battery to exhibit stiff system behavior.
28 Continuous-time identification reduces the sensitivity of the model parametrization in case of a
29 stiff dynamic system, leading to improvements on battery parameter estimation in simulation and
30 experiment results, especially when battery dynamic parameters are stored in fixed precision.
31
32
33
34
35

36 The general modeling of both continuous-time and discrete-time n^{th} -order ECM is first dis-
37 cussed. Then it is shown that the n^{th} -order ECM is identifiable if the order of the time-constants
38 is strictly defined. The comparison between continuous-time and discrete-time methods indicates
39 that discrete-time identification methods are less robust due to undesired sensitivity issues in trans-
40 formation of discrete domain parameters. In continuous-time parameter identification, SVF is used
41
42
43
44
45
46

47 **Table 3:** MAE and RMSE of model voltage estimation in whole UDDS validation.
48

	DT LS	DT LS filter	CT LSSVF	CT IVSVF
MAE [mV]	8.59	8.71	6.34	4.27
RMSE [mV]	9.35	10.36	6.96	4.95

1
2
3 to smoothen the time-derivative terms. After that, the IV method is applied to further increase the
4 estimation accuracy by reducing the correlation between equation error and regressor.
5
6

7 Simulation results show that the continuous-time identification methods demonstrate higher
8 accuracy in stiff system estimations given different sampling intervals and noise levels, because of
9 the inherent SVF pre-filtering and the avoidance of pole discretization. Characterization experi-
10 ments are conducted and different identification methods are used to identify the battery parame-
11 ters, including DT LS, DT LS with pre-filtering, CT LSSVF and CT IVSVF. The results indicate
12 that the continuous-time identification methods results in the smallest mean absolute error and
13 root mean square error. Among all, the best output voltage prediction is obtained by CT IVSVF
14 method.
15
16
17
18
19
20
21

22 This research bridges the gap between battery parameter estimation algorithm development
23 and real applications, where the system is stiff and the storage resolutions are limited. It is im-
24 portant to note that the offline continuous-time parameter estimation can be easily adapted online.
25 With a more accurate battery model, the estimation of other battery states can be improved accord-
26 ingly, such as SoC, SoH and SoP. The future work includes the implementation of the improved
27 recursive continuous-time system identification methods to battery online state estimation.
28
29
30
31
32
33
34

35 **Acknowledgement**

36
37
38 The authors would like to acknowledge the funding support from Nanjing Golden Dragon
39 Bus Co., Ltd., and the US Department of Energy under the Graduate Automotive Technology
40 Education Center program.
41
42
43
44

45 **References**

- 46
47
48 [1] L. Lu, X. Han, J. Li, J. Hua, M. Ouyang, A review on the key issues for lithium-ion battery management in
49 electric vehicles, *Journal of power sources* 226 (2013) 272–288.
50
51 [2] X. Hu, S. Li, H. Peng, A comparative study of equivalent circuit models for li-ion batteries, *Journal of Power*
52 *Sources* 198 (2012) 359–367.
53
54 [3] F. Sun, R. Xiong, A novel dual-scale cell state-of-charge estimation approach for series-connected battery pack
55 used in electric vehicles, *Journal of Power Sources* 274 (2015) 582–594.
56
57
58

- 1
2
3
4 [4] M. A. Monem, K. Trad, N. Omar, O. Hegazy, B. Mantels, G. Mulder, P. Van den Bossche, J. Van Mierlo,
5 Lithium-ion batteries: Evaluation study of different charging methodologies based on aging process, *Applied*
6 *Energy* 152 (2015) 143–155.
7
8 [5] R. Xiong, F. Sun, Z. Chen, H. He, A data-driven multi-scale extended kalman filtering based parameter and state
9 estimation approach of lithium-ion olymer battery in electric vehicles, *Applied Energy* 113 (2014) 463–476.
10
11 [6] X. Han, M. Ouyang, L. Lu, J. Li, A comparative study of commercial lithium ion battery cycle life in electric
12 vehicle: Capacity loss estimation, *Journal of Power Sources* 268 (2014) 658–669.
13
14 [7] Z. Chen, B. Xia, C. C. Mi, R. Xiong, Loss-minimization-based charging strategy for lithium-ion battery, *Industry*
15 *Applications, IEEE Transactions on* 51 (5) (2015) 4121–4129.
16
17 [8] F. Sun, R. Xiong, H. He, A systematic state-of-charge estimation framework for multi-cell battery pack in
18 electric vehicles using bias correction technique, *Applied Energy* 162 (2016) 1399–1409.
19
20 [9] A. Seaman, T.-S. Dao, J. McPhee, A survey of mathematics-based equivalent-circuit and electrochemical battery
21 models for hybrid and electric vehicle simulation, *Journal of Power Sources* 256 (2014) 410–423.
22
23 [10] C. Fleischer, W. Waag, H.-M. Heyn, D. U. Sauer, On-line adaptive battery impedance parameter and state esti-
24 mation considering physical principles in reduced order equivalent circuit battery models: Part 1. requirements,
25 critical review of methods and modeling, *Journal of Power Sources* 260 (2014) 276–291.
26
27 [11] M. Chen, G. A. Rincon-Mora, Accurate electrical battery model capable of predicting runtime and I-V perfor-
28 mance, *IEEE Transactions on Energy Conversion* 21 (2) (2006) 504–511.
29
30 [12] B. Fridholm, T. Wik, M. Nilsson, Robust recursive impedance estimation for automotive lithium-ion batteries,
31 *Journal of Power Sources* 304 (2016) 33–41.
32
33 [13] X. Tang, X. Mao, J. Lin, B. Koch, Li-ion battery parameter estimation for state of charge, in: *American Control*
34 *Conference (ACC), San Francisco, 2011*, pp. 941–946.
35
36 [14] T. Kim, Y. Wang, H. Fang, Z. Sahinoglu, T. Wada, S. Hara, W. Qiao, Model-based condition monitoring for
37 lithium-ion batteries, *Journal of Power Sources* 295 (2015) 16–27.
38
39 [15] B. Xia, C. Chen, Y. Tian, M. Wang, W. Sun, Z. Xu, State of charge estimation of lithium-ion batteries based on
40 an improved parameter identification method, *Energy* 90 (2015) 1426–1434.
41
42 [16] H. Garnier, M. Mensler, A. Richard, Continuous-time model identification from sampled data: implementation
43 issues and performance evaluation, *International Journal of Control* 76 (13) (2003) 1337–1357.
44
45 [17] J. Remmlinger, M. Buchholz, M. Meiler, P. Bernreuter, K. Dietmayer, State-of-health monitoring of lithium-
46 ion batteries in electric vehicles by on-board internal resistance estimation, *Journal of Power Sources* 196 (12)
47 (2011) 5357–5363.
48
49 [18] H. Garnier, P. C. Young, The advantages of directly identifying continuous-time transfer function models in
50 practical applications, *International Journal of Control* 87 (7) (2014) 1319–1338.
51
52 [19] G. P. Rao, N. K. Sinha, Continuous-time models and approaches, in: *Identification of continuous-time systems*,

- 1
2
3 Springer, 1991, pp. 1–15.
4
5 [20] H. Wu, S. Yuan, X. Zhang, C. Yin, X. Ma, Model parameter estimation approach based on incremental analysis
6 for lithium-ion batteries without using open circuit voltage, *Journal of Power Sources* 287 (2015) 108–118.
7
8 [21] S. Yuan, H. Wu, X. Ma, C. Yin, Stability analysis for li-ion battery model parameters and state of charge
9 estimation by measurement uncertainty consideration, *Energies* 8 (8) (2015) 7729–7751.
10
11 [22] H. Garnier, L. Wang (Eds.), *Identification of continuous-time models from sampled data*, Springer, London,
12 2008.
13
14 [23] H. Garnier, *Direct continuous-time approaches to system identification. Overview and benefits for practical*
15 *applications*, *European Journal of Control* 24 (2015) 50–62.
16
17 [24] H. Garnier, R. R. Bitmead, R. de Callafon, *Direct continuous-time model identification of high-powered light-*
18 *emitting diodes from rapidly sampled thermal step response data*, in: *19th Triennial IFAC World Congress on*
19 *Automatic Control*, Cape Town, South Africa, 2014.
20
21 [25] G. Rao, H. Unbehauen, *Identification of continuous-time systems*, in: *Control Theory and Applications, IEE*
22 *Proceedings-*, Vol. 153, 2006.
23
24 [26] K. Godfrey, J. DiStefano III, *Identifiability of model parameters, Identifiability of parametric models* (1987)
25 1–20.
26
27 [27] R. Bellman, K. J. Åström, *On structural identifiability*, *Mathematical biosciences* 7 (3) (1970) 329–339.
28
29 [28] S. M. Alavi, A. Mahdi, S. J. Payne, D. A. Howey, *Structural identifiability of battery equivalent circuit models*,
30 *arXiv preprint arXiv:1505.00153*.
31
32 [29] J. Jiang, Q. Liu, C. Zhang, W. Zhang, *Evaluation of acceptable charging current of power li-ion batteries based*
33 *on polarization characteristics*, *Industrial Electronics, IEEE Transactions on* 61 (12) (2014) 6844–6851.
34
35 [30] P. C. Young, *Recursive estimation and time-series analysis: An introduction for the student and practitioner*,
36 *second edition*, Springer-Verlag, Berlin, 2011.
37
38 [31] S. Nejad, D. Gladwin, D. Stone, *A systematic review of lumped-parameter equivalent circuit models for real-*
39 *time estimation of lithium-ion battery states*, *Journal of Power Sources* 316 (2016) 183–196.
40
41
42
43
44
45
46
47
48
49
50
51
52
53
54
55
56
57
58
59
60
61
62
63
64
65